Journal of Non-Crystalline Solids 533 (2020) 119941

Contents lists available at ScienceDirect

Journal of Non-Crystalline Solids

journal homepage: www.elsevier.com/locate/jnoncrysol

Thermal, structural and soft magnetic properties of FeSiBPCCu alloys

Xingdu Fan[a], Mufeng Jiang[a,b], Tao Zhang[a], Long Hou[a], Chaoxiang Wang[a], Baolong Shen[a,c,*]

[a] Jiangsu Key Laboratory for Advanced Metallic Materials, School of Materials Science and Engineering, Southeast University, Nanjing 211189, PR China
[b] Londerful New Material Technology Corp., Nantong 226233, PR China
[c] Institute of Massive Amorphous Metal Science, China University of Mining and Technology, Xuzhou 221116, PR China

ARTICLE INFO

Keywords:
Nanocrystalline alloy
Thermal stability
Microstructure
Soft magnetic properties

ABSTRACT

Lower Si and C-content $Fe_{83.3}Si_2B_{13-x}P_xC_1Cu_{0.7}$ alloys were prepared in order to investigate the influence of P substitution on thermal, structural and soft magnetic properties. Thermodynamic investigation reveals that proper P addition not only favors the amorphous formation but also expands the crystallization window and inactivates the annealing sensitivity of alloys. Microstructure and X-ray photoelectron spectroscopy analysis indicate P addition facilitates homogeneous precipitation of α-Fe nanocrystals but results in the formation of loose packing structure, favors the *p-d* hybridization and promotes the annihilation of effective magnetic moments of Fe atoms, leading to the decrease in saturation magnetic flux density (B_s) of amorphous phase. By proper isothermally annealing, the $Fe_{83.3}Si_2B_9P_4C_1Cu_{0.7}$ nanocrystalline alloy was developed combined with high B_s of 1.78 T, low coercivity of 4.6 A/m, and high permeability of 15100.

1. Introduction

Over the past decade, nanocrystalline FeSiBPCu alloys (NANOMET) have got much attention for their outstanding comprehensive soft magnetic properties (SMPs), including high magnetic flux density (B) of 1.8–1.94 T which is close to that of oriented silicon steels and ultra-low core loss with only ~1/3 of the latter at power frequency [1–3]. Being free of precious metal elements i.e. Nb, Co, Ge, etc., the NANOMET alloys also possess an advantage of low material cost compared with traditional nanocrystalline alloys [4–7]. However, the amorphous forming ability (AFA) of NANOMET is relatively poor, as they can only be prepared into amorphous ribbons and the thickness has to be suppressed to < 20 μm, which limits their applications. Therefore, how to improve the AFA has become the principal matter for NANOMET alloys.

Very recently, our group has successfully developed novel $Fe_{83.3}Si_4B_8P_{4-x}C_xCu_{0.7}$ alloys with high AFA and good SMPs by minor C doping. The increase in AFA is associated with lower melting entropy, the approaching to eutectic and micro-alloying effect [8]. Nevertheless, the substitution of C element on the expense of P will deteriorate the SMPs to a certain extent, as it has been reported that P exerts an important influence on SMPs of NANOMET-type alloys by easily inducing the Cu-P clusters during quenching [9], which possibly can provide nucleation sites for α-Fe grains and consequently lead to a homogeneous structure with good SMPs [8–11]. Meanwhile, it has been proved that Si element is favorable to obtain a finer and more uniform nanostructure with less strict annealing treatment, since the addition of Si can significantly stabilize the thermal stability of residual amorphous phase [12]. However, excessive Si addition also leads to large local field-induced magnetic anisotropy, especially when the crystallization volume fraction (V_{cry}) is particularly large, which deteriorates the SMPs [13]. Therefore, on the balance between thermal stability and SMPs, lower Si and C-containing $Fe_{83.3}Si_2B_{13-x}P_xC_1Cu_{0.7}$ alloys were prepared with the aim of further understanding the role of P in novel FeSiBPCCu alloy system. The influence of P doping on thermal, structural and soft magnetic properties of $Fe_{83.3}Si_2B_{13-x}P_xC_1Cu_{0.7}$ alloys was investigated.

2. Experimental procedure

Master ingots of $Fe_{83.3}Si_2B_{13-x}P_xC_1Cu_{0.7}$ (x = 0–6, denoted as P_0 to P_6, respectively) were prepared by induction melting the mixture of pure Fe (99.98 mass%), Si (99.999 mass%), B (99.5 mass%), Cu (99.99 mass%) and pre-melted Fe-P and Fe-C alloys in an Ar atmosphere. Single roller melt-spinning was used for producing alloy ribbons with ~1 mm in width and 18–40 μm in thickness. The ribbon width was mainly controlled by nozzle size while the thickness was controlled by injection pressure and linear speed of copper roller. Thermal characteristic parameters related to the melting and solidification behaviors were measured by differential scanning calorimetry (DSC, NETZSCH 404C) at a heating/cooling rate of 0.33 °C/s. Isothermal curves were measured by DSC at different isothermal temperature at a heating rate

* Corresponding author.
E-mail address: blshen@seu.edu.cn (B. Shen).

https://doi.org/10.1016/j.jnoncrysol.2020.119941
Received 30 September 2019; Received in revised form 12 January 2020; Accepted 15 January 2020

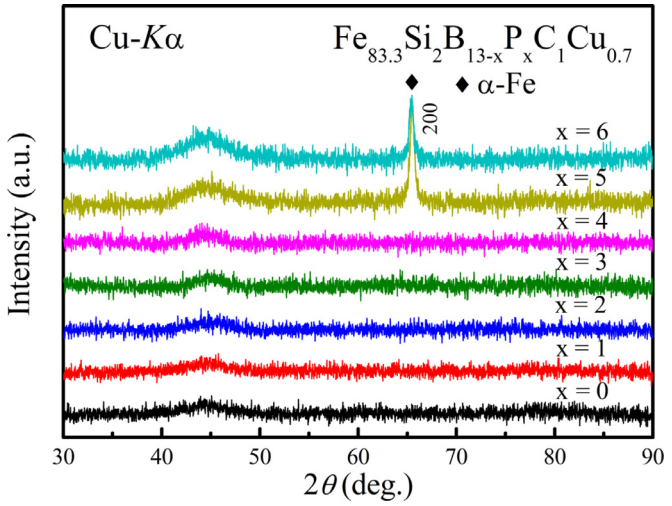

Fig. 1. XRD patterns of $Fe_{83.3}Si_2B_{13-x}P_xC_1Cu_{0.7}$ melt-spun alloys.

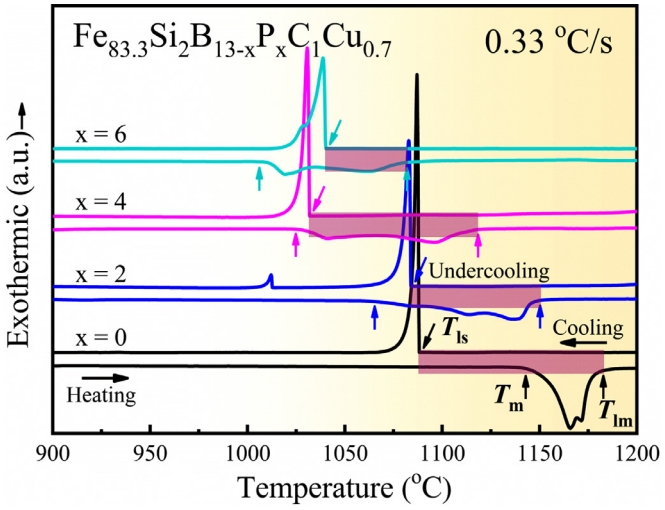

Fig. 2. DSC curves of the melting and solidification processes for $Fe_{83.3}Si_2B_{13-x}P_xC_1Cu_{0.7}$ (x = 0, 2, 4, 6) alloys at the heating/cooling rate of 0.33 °C/s. The rectangular grid areas are guides for eyes.

of 0.83 °C/s. Melt-spun ribbons were cut to ~60 mm in length for isothermal annealing. In the annealing procedure, samples were placed in a quartz tube under vacuum and then placed in a furnace preheated to the annealing temperature (T_a) for a prescribed time, followed by quench cooling in the water. Microstructures were identified by X-ray diffraction (XRD, Bruker D8-Discover) with Cu $K\alpha_1$ radiation and transmission electron microscopy (TEM, Tecnai F20). The B_s was measured by a vibrating sample magnetometer (VSM, Lake Shore 7407) under a maximum applied field of 800 kA/m while the coercivity (H_c) was measured by a *DC* B-H loop tracer (RIKEN, BHS-40) under an applied field of 1 kA/m. Effective permeability (μ_e) measurement was carried out by an impedance analyzer (Agilent 4294 A) under the field of 1 A/m. The valence-band spectra were evaluated by X-ray photoelectron spectroscopy (XPS, Thermo Scientific K-Alpha$^+$) with monochrome Al $K\alpha$ X-ray source. At least five samples of each alloy were measured to allow the determination of average values and errors for magnetic properties.

3. Results and discussion

Fig. 1 shows the XRD patterns of $Fe_{83.3}Si_2B_{13-x}P_xC_1Cu_{0.7}$ melt-spun alloys. Here, all ribbon samples (~22–24 μm thick) are measured by free-side. It is clear that the P_0 to P_4 alloys exhibit halo patterns, which indicates the amorphous structural feature. Diffraction peaks at $2\theta = 65^\circ$ corresponding to (200)-reflection of α-Fe phase are detected when P content increases to 5 and 6 at.%. This phenomenon is common in Fe-based amorphous alloys, especially those with high Fe content, which has been proved to be related to surface crystallization, because the (200)-plane is oriented parallel to the ribbon surface hence it can be easily detected [8, 14,15].

Thermal parameters of melt-spun alloys were measured in order to further understand the AFA. Fig. 2 shows the melting and solidification curves of $Fe_{83.3}Si_2B_{13-x}P_xC_1Cu_{0.7}$ (x = 0, 2, 4, 6) alloys. As can be seen, in the melting process, both the onset and offset temperatures of the melting endothermic event (denoted as T_m and T_{lm}, respectively) gradually decrease with increasing P addition whereas the solidification curve exhibits differently. Although the liquidus temperature (T_{ls}) also gradually decreases with minor P addition, the solidification exothermic peak changes from one for P_0 alloy to two for P_2 alloy, indicating a deviation of eutectic point (T_e), as P addition can easily induce the hetero-precipitation of α-Fe nanoclusters [9]. For the P_4 alloy, the existing single sharp exothermic peak again with the lowest T_{ls} indicates that the composition of this alloy is closer to T_e compared with other alloys, therefore favoring the formation of amorphous. While further increasing P addition to 6 at.%, the T_{ls} drifts to a higher temperature and the solidification exothermic peak changes from one to two again. Meanwhile, it is clear that the P_6 alloy has a smaller degree of undercooling ($\Delta T_L = T_{lm} - T_{ls}$, as shown in the rectangular grid area) than other alloys, which implies its liquid is less thermally stable during cooling and therefore has a lower AFA [16].

In order to evaluate the AFA of these alloys, we further validate the critical thickness and corresponding wheel speed for amorphous formation versus P contents, as shown in Fig. 3. It is found that the alloys with no or minor P addition possess obviously higher AFA, though there is a slight decrease in critical thickness for P_2 alloy (33 ± 1 μm) due to the deviation of T_e. On contrary, amorphous P_6 alloy must be produced under a high linear speed of ≥ 50 m/s and the critical thickness is only 18 ± 1 μm. It is noted that a good consistency can be found by comparing the variation of ΔT_L with the critical thickness and corresponding wheel speed, that is, the ΔT_L firstly decreases and then increases with minor P addition, followed by a sharp decrease from 90 °C for the P_4 alloy to 42 °C for the P_6 alloy. Accordingly, the AFA validation results are perfectly in agreement with microstructural and thermal measurements, which indicates that excessive P addition decreases the thermal stability of supercooled liquid, promotes the surface crystallization and hence deteriorates the AFA. Therefore, in order to obtain amorphous alloys with easy preparation, the critical P content is limited to 4 at.% in this alloy system.

Fig. 4 shows the DSC curve of crystallization process for

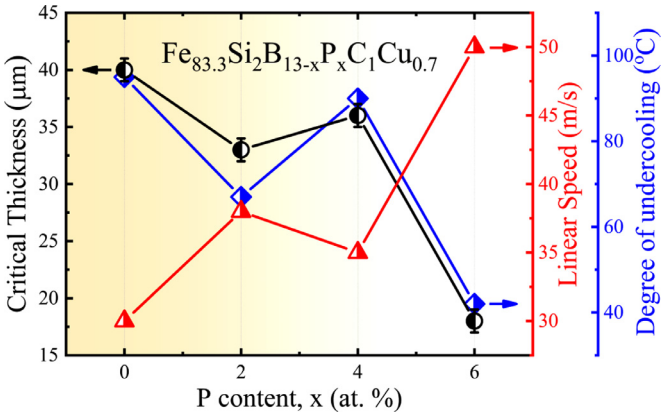

Fig. 3. The critical thickness, corresponding linear speed and degree of undercooling (ΔT_L) of alloy ribbons versus P content (x = 0, 2, 4 and 6). The dotted lines are guides for eyes.

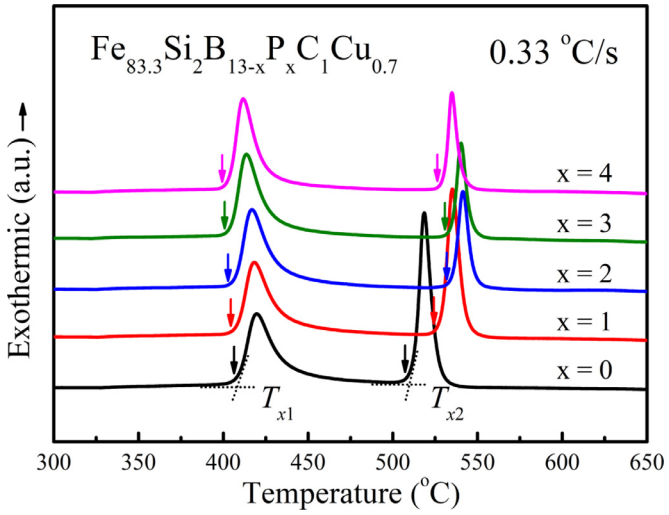

Fig. 4. DSC curve of the crystallization process for $Fe_{83.3}Si_2B_{13-x}P_xC_1Cu_{0.7}$ alloys.

$Fe_{83.3}Si_4B_8P_{4-x}C_xCu_{0.7}$ melt-spun alloy ribbons. Here, we only discuss the alloys with higher AFA (x = 0–4). It is seen that the first onset crystallization temperature (T_{x1}) gradually shifts to a lower temperature with the increase in P contents, indicating that the replacement of P for B is beneficial to the precipitation of initial α-Fe phase. Meanwhile, the crystallization temperature of second phases (T_{x2}) undergoes an obvious increase firstly and then a slight decrease, hence the crystallization interval between T_{x1} and T_{x2} is expanded by P doping, which is beneficial for annealing to achieve single α-Fe phase.

Isothermal DSC was performed on P_0 and P_4 alloys for further investigating the crystallization behavior, as illustrated in Fig. 5(a) and (c). There is an exothermic peak appearing after an incubation time (τ), which is associated with the nucleation and precipitation process of α-Fe phase [17]. The τ for P_0 and P_4 alloys is similar and shifts a little leftward as isothermal temperature rises, which means τ become shorter, while the precipitation of α-Fe phase for the latter undergoes an obviously longer period. Fig. 5(b) and (d) illustrate the dependence of V_{cry} on annealing time by integrating the area of isothermal curves between the starting and ending time of crystallization. The crystallization process exhibits a typical S-shape after a similar τ but the inclinations of curves are very different. The P_4 alloy exhibits an obviously flatter shape, which confirms a longer precipitation process of α-Fe crystals.

Fig. 6 shows the temperature-time-transformation (TTT) diagrams

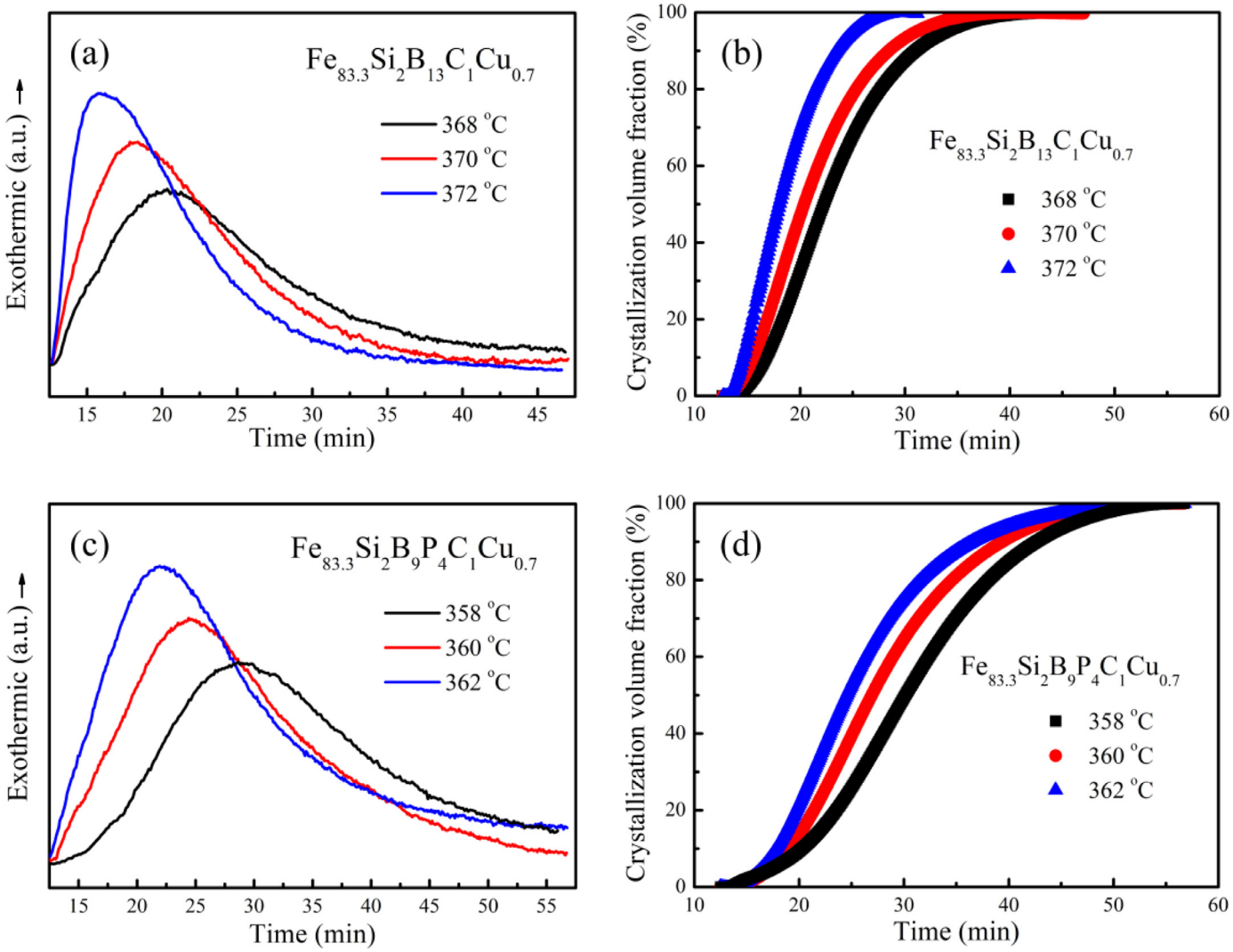

Fig. 5. Isothermal curve and corresponding crystallization volume fraction (V_{cry}) dependent on annealing time for $Fe_{83.3}Si_2B_{13-x}P_xC_1Cu_{0.7}$ melt-spun alloys with (a) and (b): x = 0, (c) and (d): x = 4, respectively.

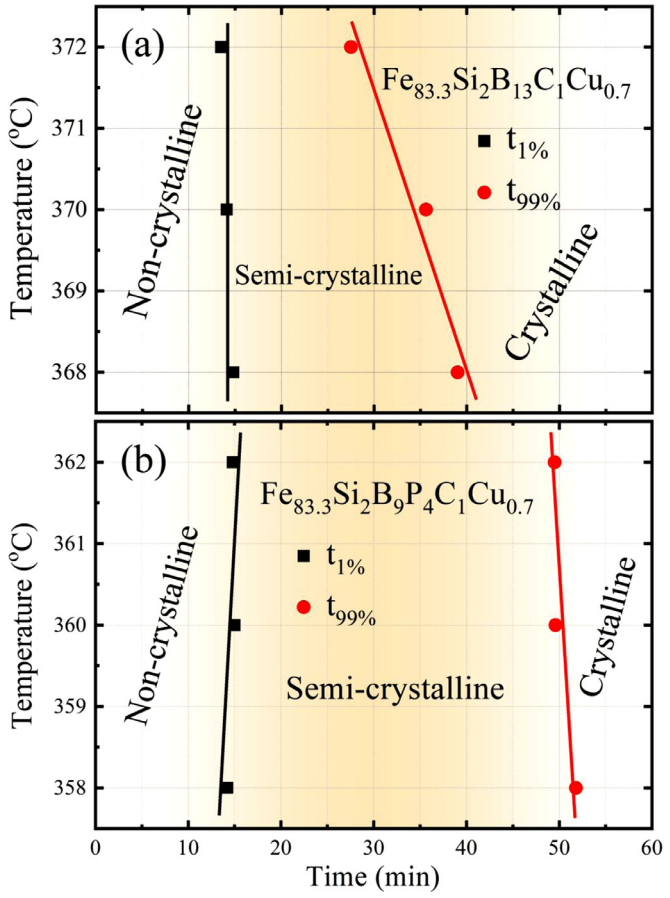

Fig. 6. Temperature-time-transformation (TTT) diagrams of $Fe_{83.3}Si_2B_{13-x}P_xC_1Cu_{0.7}$ melt-spun alloys with (a) $x = 0$ and (b) $x = 4$, respectively. The dotted lines are guides for eyes.

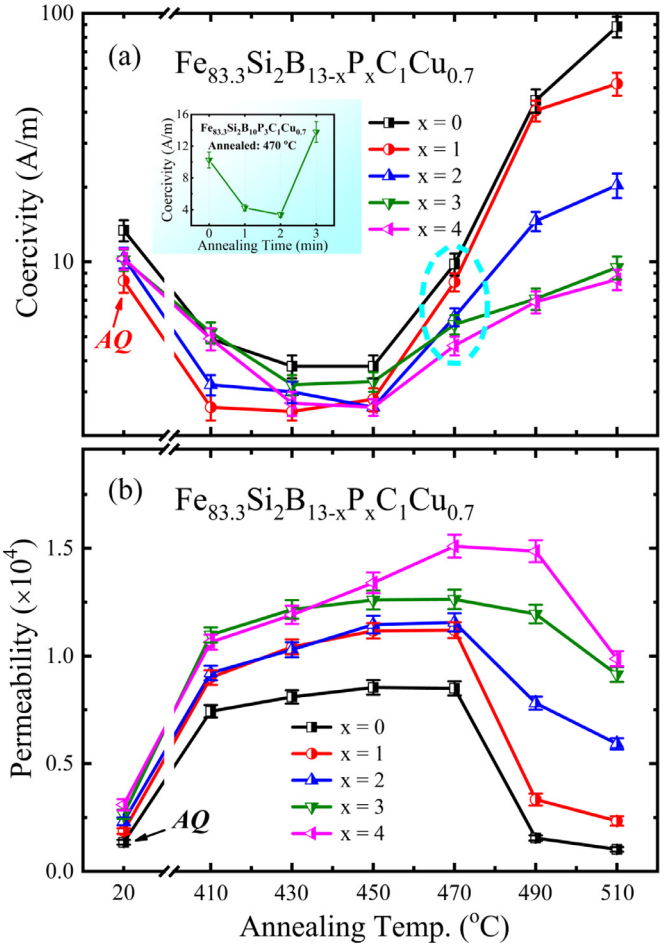

Fig. 7. The dependence of (a) coercivity (H_c) and (b) effective permeability (μ_e) on annealing temperature (T_a) of $Fe_{83.3}Si_2B_{13-x}P_xC_1Cu_{0.7}$ alloys. The inset shows the variation of H_c versus annealing time at 470 °C for $x = 3$. The dotted lines in the inset of (a) are guides for eyes.

obtained from isothermal curves. Here $t_{1\%}$ and $t_{99\%}$ stand for the time with 1% and 99% of crystallization, respectively. The diagrams were therefore divided into non-crystalline, semi-crystalline and crystalline regions [17]. In non-crystalline stage, the nucleation begins from small crystals and grows, but the V_{cry} is not considerable. On the other hand, the crystallization rate increases significantly in the semi-crystalline stage and thus it can reveal the thermal stability of crystalline phase [17]. Accordingly, the semi-crystalline region of P_4 alloy is obviously wider than that of P_0 alloy, especially at higher temperatures, indicating the α-Fe nanocrystals can be precipitated in a wide temperature and time range and confirming a better thermal stability. Taking the above thermodynamic investigation into consideration, it can be concluded that minor P addition expands the crystallization window of FeSiBPCCu alloys, inactivates their annealing sensitivity and is consequently advantageous for obtaining good SMPs.

Fig. 7(a) illustrates the dependence of H_c on T_a of $Fe_{83.3}Si_2B_{13-x}P_xC_1Cu_{0.7}$ alloys. The inset shows the variation of H_c versus annealing time at 470 °C for P_3 sample. It is obvious that H_c decreases significantly with increasing annealing time and reaches its minimum at 2 min while 3-min annealing induces a large H_c of 13.8 A/m, hence the annealing time is fixed as 2 min. Accordingly, the H_c first decreases gradually with increasing T_a and reaches each minimum at ~ 430–450 °C, which is attributed to stress release and partial crystallization. Then for P_0 and P_1 alloys, H_c increases at 470 °C and takes a dramatic increase with the further increasing T_a. The H_c for P_2 to P_4 alloys shows a similar variation, but the variation trend is much more placid, implying better thermal stability of crystalline phase. The dependence of μ_e on T_a shows an inverse variation trend (*see* Fig. 7(b)), another obvious difference is that it reaches each maximum at 470 °C, which means a higher V_{cry}.

Fig. 8(a) summarizes the dependence of B_s and H_c on P contents of $Fe_{83.3}Si_2B_{13-x}P_xC_1Cu_{0.7}$ alloys annealed at 470 °C for 2 min. According to the result, B_s shows a linear increase with increasing P content, while H_c takes an opposite variation. Hysteresis loops of the annealed $Fe_{83.3}Si_2B_{13-x}P_xC_1Cu_{0.7}$ alloys (*see* Fig. 8(b)) exhibit typical ferromagnetic features. With P substitution, B_s increases dramatically from 1.63 T for $x = 0$ to 1.78 T for $x = 4$ alloy, respectively. It has been reported that B_s is greatly associated with magnetization in crystalline (B_{sc}) and amorphous (B_{sa}) phases and can be expressed by equation $B_s = B_{sc}V_{cry} + B_{sa}(1\text{-}V_{cry})$ [8,18]. The B_{sc} is ~2.1 T for α-Fe [18], while B_{sa} can be obtained from the magnetization of melt-spun alloys, as illustrated in Fig. 8(c). It is clear that B_{sa} shows a monotonous decrease which means the increase in B_s is mainly attributed to the increasing V_{cry} of α-Fe nanocrystals. Therefore, we further analyzed the microstructure of FeSiBPCCu annealed alloys as illustrated in Fig. 8(d). A crystallization phase identified to the (110)-reflection of α-Fe superimposes on the amorphous diffusion halo for P_0 and P_1 samples, which means the precipitation amount of α-Fe is so small that the grain size (D) cannot be detected [19,20]. Increasing P addition obviously induces a large amount of α-Fe grains. The V_{cry} is 27.5 ± 2.0%, 33.1 ± 2.0% and 45.9 ± 2.1% for P_2, P_3 and P_4 alloys, respectively, indicating that P substitution significantly favors the precipitation of single α-Fe phase, which confirms the reason for B_s increasing. Meanwhile, the increase in V_{cry} also means the strengthening of exchange-coupling interaction between crystalline and amorphous phases, which effectively decreases

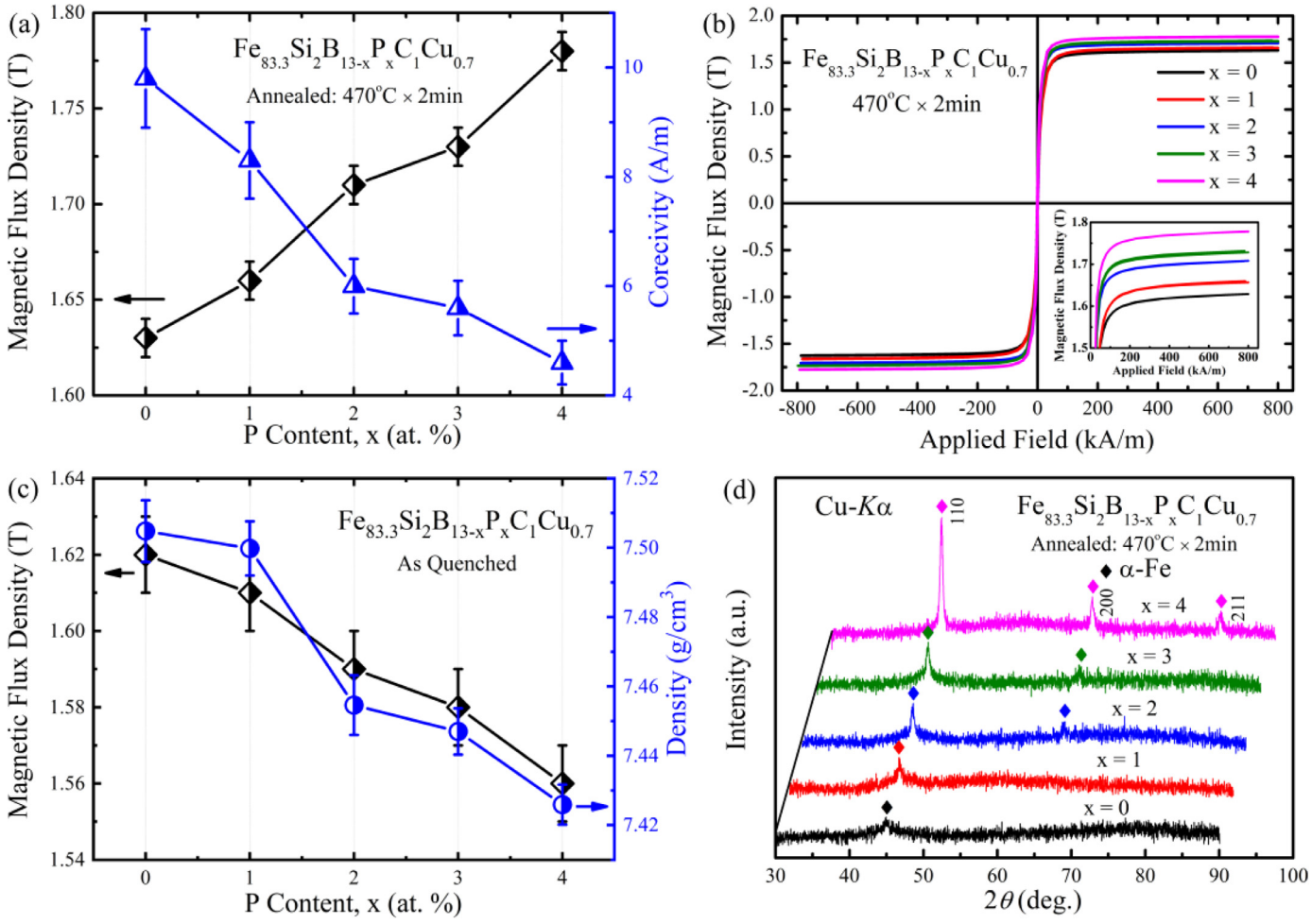

Fig. 8. Magnetic performance and microstructure of FeSiBPCCu alloys: (a) the dependence of saturation magnetic flux density (B_s) and coercivity (H_c) on P content and (b) Hysteresis loops of $Fe_{83.3}Si_2B_{13-x}P_xC_1Cu_{0.7}$ nanocrystalline alloys, (c) the dependence of B_s and density (ρ) on P content of $Fe_{83.3}Si_2B_{13-x}P_xC_1Cu_{0.7}$ melt-spun alloys and (d) XRD patterns of $Fe_{83.3}Si_2B_{13-x}P_xC_1Cu_{0.7}$ alloys annealed at 470 °C for 2 min. The dotted lines in (a) and (c) are guides for eyes.

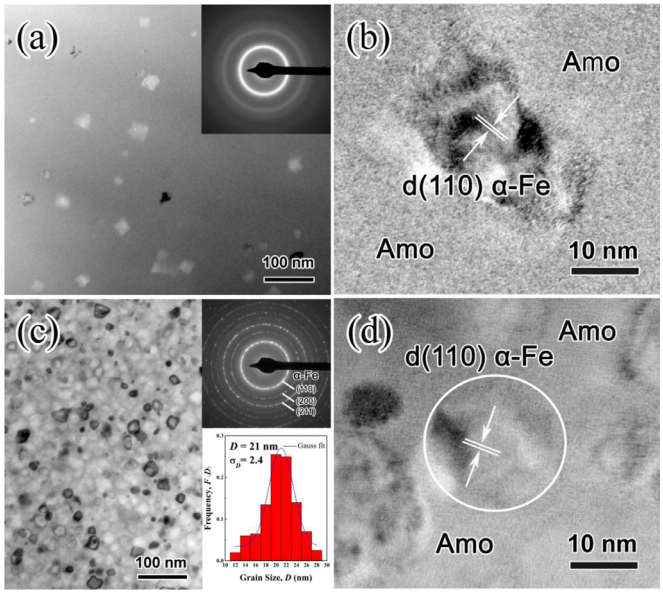

Fig. 9. The bright-field TEM images, selected area electron diffraction (SAED) patterns, grain size distribution and corresponding high resolution-TEM (HRTEM) images of $Fe_{83.3}Si_2B_{13-x}P_xC_1Cu_{0.7}$ alloys annealed at 470 °C for 2 min with (a) and (b): $x = 0$; (c) and (d): $x = 4$, respectively. The dotted line in the inset of (c) shows Gauss fit.

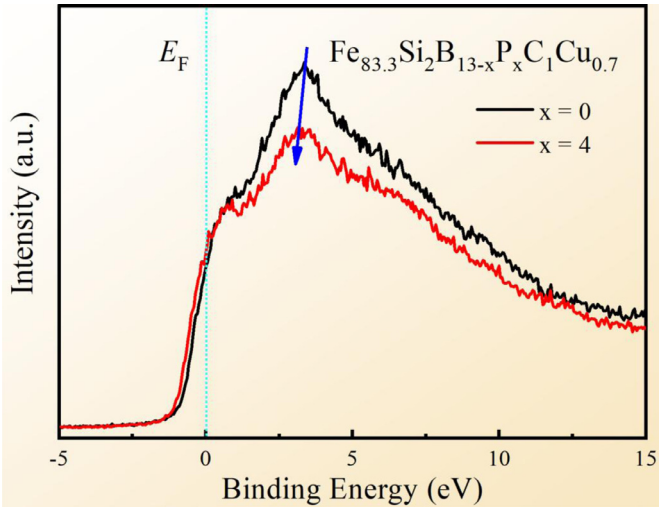

Fig. 10. XPS valence-band spectra of $Fe_{83.3}Si_2B_{13-x}P_xC_1Cu_{0.7}$ melt-spun alloys with $x = 0$ and 4.

the magneto-crystalline anisotropy ($<K>$) and therefore reduces the H_c [20–22].

Fig. 9 illustrates the bright-field TEM images and SAED patterns of $Fe_{83.3}Si_2B_{13-x}P_xC_1Cu_{0.7}$ nanocrystalline alloys with $x = 0$ and 4. The

microstructure observation reveals that annealed P_4 alloy exhibits a much denser and uniform nanostructure than P_0 alloy. The average D is ~21 nm and the number density (N_d) is ~$9.5 \times 10^{22}\ m^{-3}$, which is consistent with the literatures [8,23]. Meanwhile, HRTEM image shows that the grain morphology appears irregular for P_0 alloy, implying a larger $\langle K \rangle$ induced by oriented growth of α-Fe crystals, therefore H_c of this alloy is as high as 9.8 A/m. However, increasing P addition clearly promotes the homogeneous precipitation of α-Fe crystals, resulting in an obviously high V_{cry} and N_d. Therefore, the $\langle K \rangle$ is effectively averaged out by magnetic exchange-coupling, leading to a uniform microstructure with circular grains [20–22]. As a result, good SMPs are achieved for P_4 alloy with high B_s of 1.78 T, low H_c of 4.6 A/m and high μ_e of 15100.

It should be noted that the value of B_s for this alloy is only 1.78 T, whereas the reported B_s for NANOMET-type alloys ranges from 1.8 T to 1.94 T [1–3]. Here we explain the difference found for SMPs. As discussed above, the B_s of nanocrystalline alloys is strongly dependent on V_{cry} and composition of crystalline phase [15]. V_{cry} is mainly dominated by annealing conditions whereas the latter is determined not only by primitive composition but also the as-quenched state of ribbons. Firstly, the density (ρ) of melt-spun alloys shows an evident decrease with P substitution as illustrated in Fig. 8(c), indicating the formation of loose packing structure, which not only decreases the AFA but also weakens the exchange-coupling between Fe-Fe and Fe-metallic atoms hence decreases the B_s [24,25]. Secondly, the formation of localized *p-d* type hybrid bonds between Fe and P atoms due to the unpaired electrons in 2p/3p outer shell of P atom essentially promotes the ferro- and anti-ferro-magnetic exchange-coupling between metals and metalloids and leads to the weakening of magnetic moment [26–28]. Based on this theoretical analysis, we investigated the valence electron density of states of FeSiBPCCu melt-spun alloys with $x = 0$ and 4, as shown in Fig. 10. It is clear that each of the spectra exhibits a broad visible peak and the peak shifts nearer to the Fermi level (E_F) with binding energy from 3.48 to 3.08 eV with 4 at.% P substitution. Extensive studies revealed that the peak near E_F is closely related to the *p-d* hybridization. The closer to E_F, the stronger *p-d* hybridization will have [29,30]. Thereby, the shift of peak indicates that P substitution in FeSiBPCCu alloys favors the *p-d* hybridization to E_F and promotes the annihilation of effective magnetic moments of Fe atoms, resulting in deterioration of SMPs.

4. Conclusion

The influence of minor P substitution on amorphous formation, thermal stability microstructure and SMPs of $Fe_{83.3}Si_2B_{13-x}P_xC_1Cu_{0.7}$ alloys has been investigated. Thermodynamic investigation reveals that proper P addition favors the amorphous formation due to the improvement of thermal stability of supercooled liquid including the increase in ΔT_L, decrease in T_{ls} and the approaching to T_e, while excessive P addition promotes the surface crystallization hence deteriorates the AFA. Increasing P addition also obviously expands the crystallization window by increasing the precipitation temperature and time range of α-Fe nanocrystals and hence promotes the homogeneous precipitation of α-Fe nanocrystals, resulting in a uniform nanostructure with high V_{cry} and N_d. However, the P substitution for B also decreases the density of melt-spun alloys by inducing loose packing structure, favors the local *p-d* hybridization near E_F and promotes the annihilation of effective magnetic moments of Fe atoms, which deteriorates the SMPs. After proper annealing, B_s increases linearly with increasing P content while H_c takes an opposite variation. The $Fe_{83.3}Si_2B_9P_4C_1Cu_{0.7}$ nanocrystalline alloy is successfully prepared with high B_s of 1.78 T, low H_c of 4.6 A/m and high μ_e of 15100. The combination of high AFA and good SMPs promises the potential applications in industrial magnetic devices.

CRediT authorship contribution statement

Xingdu Fan: Conceptualization, Investigation, Writing - original draft, Writing - review & editing. **Mufeng Jiang:** Investigation. **Tao Zhang:** Investigation. **Long Hou:** Investigation. **Chaoxiang Wang:** Investigation. **Baolong Shen:** Conceptualization, Supervision, Writing - review & editing.

Declaration of Competing Interest

The authors declare that they have no known competing financial interests or personal relationships that could have appeared to influence the work reported in this paper.

Acknowledgments

This work was supported by the National Key Research and Development Program of China(Grant No. 2016YFB0300502), the National Natural Science Foundation of China (Grant Nos. 51631003 and 51871237) and the Fundamental Research Funds for the Central Universities (Grant Nos. 2242018K40112 and 2242019K40062).

References

[1] A. Makino, H. Men, T. Kubota, K. Yubuta, A. Inoue, FeSiBPCu nanocrystalline soft magnetic alloys with high B_s of 1.9 T produced by crystallizing hetero-amorphous phase, Mater. Trans. JIM 50 (2009) 204–209, https://doi.org/10.2320/matertrans.MER2008306.

[2] A. Makino, T. Kubota, K. Yubuta, A. Inoue, A. Urata, H. Matsumoto, S. Yoshida, Low core losses and magnetic properties of $Fe_{85-86}Si_{1-2}B_8P_4Cu_1$ nanocrystalline alloys with high B for power applications (invited), J. Appl. Phys. 109 (2011) 07A302, https://doi.org/10.1063/1.3535169.

[3] T. Kubota, A. Makino, A. Inoue, Low core loss of $Fe_{85}Si_2B_8P_4Cu_1$ nanocrystalline alloys with high B_s and B_{800}, J. Alloys Compd. 509 (2011) S416–S419, https://doi.org/10.1016/j.jallcom.2010.11.012.

[4] Y. Yoshizawa, S. Oguma, K. Yamauchi, New Fe-based soft magnetic alloys composed of ultrafine grain structure, J. Appl. Phys. 64 (1988) 6044–6046, https://doi.org/10.1063/1.342149.

[5] K. Suzuki, A. Makino, A. Inoue, T. Masumoto, Soft magnetic properties of nanocrystalline bcc Fe-Zr-B and Fe-M-B-Cu (M = transition metal) alloys with high saturation magnetization (invited), J. Appl. Phys. 70 (1991) 6232–6237, https://doi.org/10.1063/1.350006.

[6] M.A. Willard, D.E. Laughlin, M.E. McHenry, Structure and magnetic properties of $(Fe_{0.5}Co_{0.5})_{88}Zr_7B_4Cu_1$ nanocrystalline alloys, J. Appl. Phys. 84 (1998) 6773–6777, https://doi.org/10.1063/1.369007.

[7] L. Zhang, Z. Wang, Y.R. Jia, Microstructure and soft magnetic properties of $(Fe_{0.9}Co_{0.1})_{73.5}Si_{13.5}B_{9-x}Nb_3Cu_1Ge_x$ nanocrystalline alloys, Mater. Sci. Eng. B 231 (2018) 1–4, https://doi.org/10.1016/j.mseb.2017.12.028.

[8] X.D. Fan, T. Zhang, M.F. Jiang, W.M. Yang, B.L. Shen, Synthesis of novel FeSiBPCCu alloys with high amorphous forming ability and good soft magnetic properties, J. Non-Cryst. Solids 503-504 (2019) 36–43, https://doi.org/10.1016/j.jnoncrysol.2018.09.021.

[9] A. Makino, Nanocrystalline soft magnetic Fe-Si-B-P-Cu alloys with high B of 1.8-1.9T contributable to energy saving, IEEE Trans. Magn. 48 (2012) 1331–1335, https://doi.org/10.1109/TMAG.2011.2175210.

[10] M. Matsuura, Y. Zhang, M. Nishijima, A. Makino, Role of P in nanocrystallization of $Fe_{85}Si_2B_8P_4Cu_1$, IEEE Trans. Magn. 50 (2014) 2003304, , https://doi.org/10.1109/TMAG.2013.2285247.

[11] J. Xu, Y.Z. Yang, W. Li, X.C. Chen, Z.W. Xie, Effect of P addition on glass forming ability and soft magnetic properties of melt-spun FeSiBCuC alloy ribbons, J. Magn. Magn. Mater. 417 (2016) 291–293, https://doi.org/10.1016/j.jmmm.2016.05.103.

[12] Z.Q. Zhang, P. Sharma, A. Makino, Role of Si in high B_s and low core-loss $Fe_{85.2}B_{10-x}P_4Cu_{0.8}Si_x$ nano-crystalline alloys, J. Appl. Phys. 112 (2012) 103902, , https://doi.org/10.1063/1.4765718.

[13] R. Parsons, J.S. Garitaonandia, T. Yanai, K. Onodera, H. Kishimoto, A. Kato, K. Suzuki, Effect of Si on the field-induced anisotropy in Fe-rich nanocrystalline soft magnetic alloys, J. Alloys Compd. 695 (2017) 3156–3162, https://doi.org/10.1016/j.jallcom.2016.11.330.

[14] F.G. Chen, Y.G. Wang, Investigation of glass forming ability, thermal stability and soft magnetic properties of melt-spun $Fe_{83}P_{16-x}Si_xCu_1$ (x = 0, 1, 2, 3, 4, 5) alloy ribbons, J. Alloys Compd. 584 (2014) 377–380, https://doi.org/10.1016/j.jallcom.2013.09.089.

[15] E. Lopatina, I. Soldatov, V. Budinsky, M. Marsilius, L. Schultz, G. Herzer, R. Schäfer, Surface crystallization and magnetic properties of $Fe_{84.3}Cu_{0.7}Si_4B_8P_3$ soft magnetic ribbons, Acta Mater. 96 (2015) 10–17, https://doi.org/10.1016/j.actamat.2015.05.051.

[16] M. Yang, X.J. Liu, Y. Wu, H. Wang, X.Z. Wang, Z.P. Lu, Unusual relation between glass-forming ability and thermal stability of high-entropy bulk metallic glasses,

Mater. Res. Lett. 6 (2018) 495–500, https://doi.org/10.1080/21663831.2018.1482839.
[17] H.R. Lashgari, Z. Chen, X.Z. Liao, D. Chu, M. Ferry, S. Li, Thermal stability, dynamic mechanical analysis and nanoindentation behavior of FeSiB(Cu) amorphous alloys, Mater. Sci. Eng. A 626 (2015) 480–499, https://doi.org/10.1016/j.msea.2014.12.097.
[18] M. Ohta, Y. Yoshizawa, Magnetic properties of nanocrystalline $Fe_{82.65}Cu_{1.35}Si_xB_{16-x}$ alloys (x = 0-7), Appl. Phys. Lett. 91 (2007) 062517, , https://doi.org/10.1063/1.2769956.
[19] X.D. Fan, H. Men, A.B. Ma, B.L. Shen, Soft magnetic properties in $Fe_{84-x}B_{10}C_6Cu_x$ nanocrystalline alloys, J. Magn. Magn. Mater. 326 (2013) 22–27, https://doi.org/10.1016/j.jmmm.2012.08.045.
[20] X.D. Fan, Y.T. Tang, Z.X. Shi, M.F. Jiang, B.L. Shen, The effect of Ni addition on microstructure and soft magnetic properties of FeCoZrBCu nanocrystalline alloys, AIP Adv. 7 (2017) 056107, , https://doi.org/10.1063/1.4977229.
[21] G. Herzer, Grain size dependence of coercivity and permeability in nanocrystalline ferromagnets, IEEE Trans. Magn. 26 (1990) 1397–1402, https://doi.org/10.1109/20.104389.
[22] G. Hezer, Modern soft magnets amorphous and nanocrystalline materials, Acta Mater. 67 (2013) 718–734, https://doi.org/10.1016/j.actamat.2012.10.040.
[23] P. Sharma, X. Zhang, Y. Zhang, A. Makino, Competition driven nanocrystallization in high B_s and low core loss Fe-Si-B-P-Cu soft magnetic alloys, Scripta Mater. 95 (2015) 3–6, https://doi.org/10.1016/j.scriptamat.2014.08.023.
[24] C.L. Zhao, A.D. Wang, S.Q. Yue, T. Liu, A.N. He, C.T. Chang, X.M. Wang, C.T. Liu, Significant improvement of soft magnetic properties for Fe(Co)BPSiC amorphous alloys by magnetic field annealing, J. Alloys Compd. 742 (2018) 220–225, https://doi.org/10.1016/j.jallcom.2018.01.311.
[25] H.X. Li, Z.C. Lu, S.L. Wang, Y. Wu, Z.P. Lu, Fe-based bulk metallic glasses: glass formation, fabrication, properties and applications, Prog. Mater. Sci. 103 (2019) 235–318, https://doi.org/10.1016/j.pmatsci.2019.01.003.
[26] Z.M. Stadnik, G. Stroink, Electronic structure and magnetism of transition metal-metalloid glasses, J. Non-Crystal. Solids 99 (1988) 233–243, https://doi.org/10.1016/0022-3093(88)90433-4.
[27] W. Jiao, X.L. Wang, S. Lan, S.P. Pan, Z.P. Lu, Propensity of bond exchange as a window into the mechanical properties of metallic glasses, Appl. Phys. Lett. 106 (2015) 061910, , https://doi.org/10.1063/1.4908122.
[28] S. Das, K. Choudhary, A. Chernatynskiy, H.C. Yim, A.K. Bandyopadhyay, S. Mukherjee, Spin-exchange interaction between transition metals and metalloids in soft-ferromagnetic metallic glasses, J. Phys-Condens. Mat. 28 (2016) 216003, , https://doi.org/10.1088/0953-8984/28/21/216003.
[29] W.M. Yang, H.S. Liu, Y.C. Zhao, A. Inoue, K.M. Jiang, J.T. Huo, H.B. Ling, Q. Li, B.L. Shen, Mechanical properties and structural features of novel Fe-based bulk metallic glasses with unprecedented plasticity, Sci. Rep. 4 (2014) 6233–6237, https://doi.org/10.1038/srep06233.
[30] H.X. Li, C.Q. Li, D. Cao, W.M. Yang, Q. Li, Z.P. Lu, Influences of oxygen on plastic deformation of a Fe-based bulk metallic glass, Scripta Mater. 135 (2017) 24–28, https://doi.org/10.1016/j.scriptamat.2017.03.018.